# The great effect of magnetic $Fe^{2+}$ ions on electromagnetic behavior in the $Cu_{1-x}Fe_xIr_2S_4$ system



2009 J. Phys.: Condens. Matter 21 026021

(http://iopscience.iop.org/0953-8984/21/2/026021)

J. Phys.: Condens. Matter **21** (2009) 026021 (7pp) doi:10.1088/0953-8984/21/2/026021

# The great effect of magnetic $Fe^{2+}$ ions on electromagnetic behavior in the $Cu_{1-x}Fe_xIr_2S_4$ system

**Lei Zhang[1], Langsheng Ling[1], Shun Tan[1], Li Pi[1,2,4], Ning Liu[1,3] and Yuheng Zhang[1]**

[1] National High Magnetic Field Laboratory, University of Science and Technology of China, Hefei 230026, People's Republic of China
[2] Hefei National Laboratory for Physical Sciences at Microscale, University of Science and Technology of China, Hefei 230026, People's Republic of China
[3] Department of Physics, Suzhou Normal College, Suzhou 234000, People's Republic of China

E-mail: pili@ustc.edu.cn

Received 21 August 2008, in final form 13 November 2008
Published 11 December 2008
Online at stacks.iop.org/JPhysCM/21/026021

**Abstract**

The substitution of magnetic $Fe^{2+}$ for nonmagnetic $Cu^{+}$ in the $Cu_{1-x}Fe_xIr_2S_4$ system causes drastic changes in electromagnetic behavior. For $x = 0.01$ and 0.025, the Peierls-like phase transition step $\Delta M$ in magnetization increases with $x$ increasing, and an unexpected spin transition occurs at $T^* \approx 120$ K. This may be attributed to the spin-polarization of the $Ir^{4+}$ ions by the $Fe^{2+}$ ions. When $x$ exceed 0.1, the Peierls-like phase transition is suppressed completely. The magnetic state for Fe doped samples transforms from ferromagnetic (FM) to paramagnetic (PM), and back to the FM state again with the increase of $x$. For the highly doped samples, the FM domains formed by $Fe^{2+}$ ions result in another transition at $T^{**} \approx 110$ K and the cluster–spin glass transition.

(Some figures in this article are in colour only in the electronic version)

## 1. Introduction

The spinel structure compound $CuIr_2S_4$, with Cu occupying the A sites (tetrahedral) and Ir occupying the B (octahedral) sites, has been extensively studied in recent years due to the Peierls-like phase transition [1–5]. Upon cooling, the first-order metal–insulator transition happens at $T_{MI} \approx 230$ K, accompanied by an increase of about three orders of magnitude in resistivity, and an abrupt drop of magnetization due to the magnetic transition from Pauli paramagnetism to diamagnetism. Meanwhile, the lattice structure changes from cubic in the high temperature metallic phase (HMP) to tetragonal in the low temperature insulating phase (LIP) along with a reduction of 0.7% in volume ($c/\sqrt{2}a = 1.03$ in LIP); it undergoes simultaneous complex charge-ordering of the octamer and spin-dimerization transition of $Ir^{4+}$ ions [2, 6, 7]. The valence of Cu ions in the A sites is +1 [8–10], while the average valence of Ir ions in the B sites is +3.5 in HMP [4, 7].

The substitution in the A sites has been found to cause many interesting results in the $CuIr_2S_4$ system. For examples, the Peierls-like phase transition is suppressed and superconductivity is induced in $Cu_{1-x}Zn_xIr_2S_4$ [11–13]; the first-order transition is changed into a high-order transition associated with an electronic transformation from small polarons to small bipolarons in $Cu_{1-x}In_xIr_2S_4$ [14]; $Cu_{1-x}Cd_xIr_2S_4$ exhibits a miscibility-gap behavior [15]; the localized magnetic moment indicates the antiferromagnetic (AFM) negative Weiss temperature $\theta$ even in the metallic state in $Cu_{1-x}Mn_xIr_2S_4$ and $Cu_{1-x}Ni_xIr_2S_4$ [16, 17].

In this work, we choose Fe ions to replace Cu because the introduction of Fe ions in A sites in the $CuIr_2S_4$ system not only affects the proportion of $Ir^{3+}$ to $Ir^{4+}$, but also brings in localized magnetic moments. These effects should have large impact on the Peierls-like transition and electromagnetic behaviors.

[4] Author to whom any correspondence should be addressed.

 

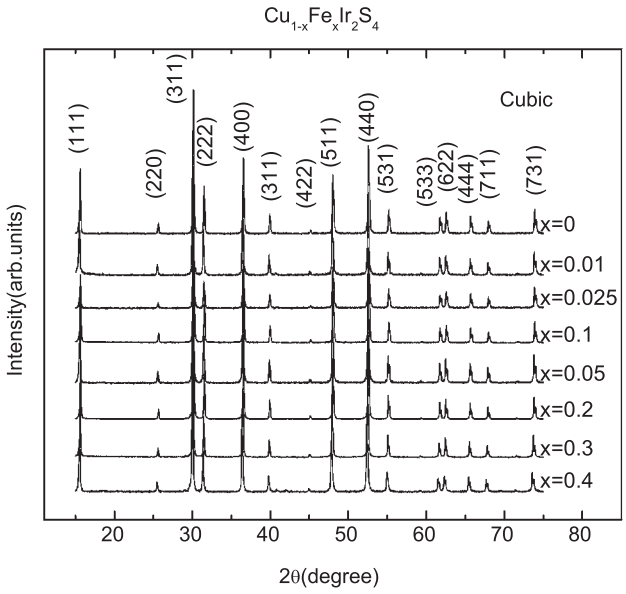


**Figure 1.** Powder x-ray diffraction (XRD) patterns for $Cu_{1-x}Fe_xIr_2S_4$ ($x = 0$, 0.01, 0.025, 0.05, 0.1, 0.2, 0.3, 0.4) at room temperature. The indices of the crystallographic plane of the diffraction peaks are marked in brackets.

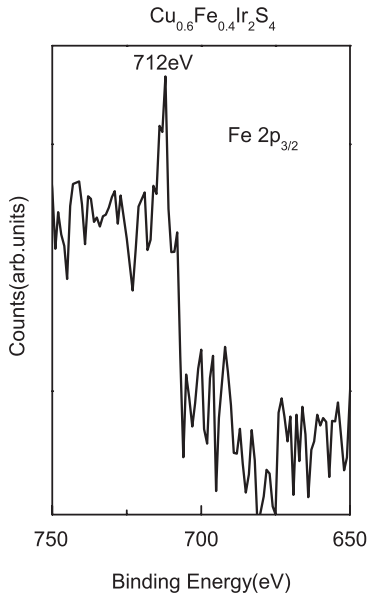


**Figure 2.** The XPS spectrum of Fe $2p_{3/2}$ for $Cu_{0.6}Fe_{0.4}Ir_2S_4$ at room temperature.

## 2. Experimental details

Polycrystalline samples $Cu_{1-x}Fe_xIr_2S_4$ ($x = 0$, 0.01, 0.025, 0.05, 0.1, 0.2, 0.3 and 0.4) were prepared by the solid state reaction method. The starting materials, high purity powders of Cu, Fe, Ir, and S were mixed in the stoichiometric ratio with 1 wt% excess S. The mixed powder samples were sealed in vacuum quartz tubes and heated to 1123 K at a rate of 100 K $h^{-1}$ for 8 days. Then, the samples were pressed into pellets, and sintered in vacuum quartz tubes again at 1173 K for 2 days.

The structure and phase purity were checked by x-ray diffraction (XRD) using a Rigaku-D/max-$\gamma A$ diffractometer employing high-intensity Cu K$\alpha$ radiation. The x-ray photoelectron spectroscopy (XPS) spectrum of Fe $2p_{3/2}$ in $Cu_{0.6}Fe_{0.4}Ir_2S_4$ was measured at room temperature to elucidate the valence of Fe. The resistivity data were collected by the conventional four-probe method. The magnetic properties were measured by a superconductive quantum interference device (SQUID) MPMS system. Electron spin resonance (ESR) spectra at different temperatures were measured using a Brucker ER200D spectrometer at 9.06 GHz.

## 3. Results and discussion

### *3.1. Structural properties*

XRD patterns at room temperature confirm that our $Cu_{1-x}Fe_xIr_2S_4$ samples with $x \leqslant 0.4$ are single phase, as shown in figure 1. The structure at room temperature is cubic with the space group of $Fd\bar{3}m$. The XPS spectrum of Fe $2p_{3/2}$ in $Cu_{0.6}Fe_{0.4}Ir_2S_4$ at room temperature is shown in figure 2. The binding energy at the peak is 712 eV which indicates that the valence of Fe ions is +2 in $Cu_{1-x}Fe_xIr_2S_4$ [18].

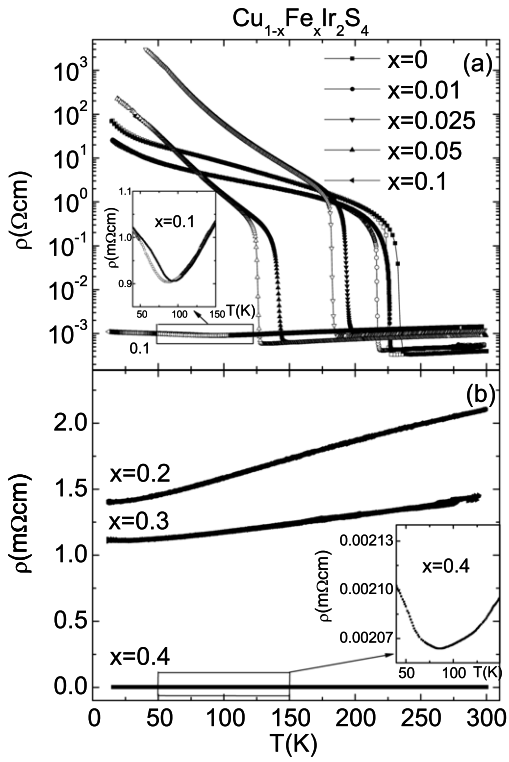


**Figure 3.** The temperature dependence of resistivity for $Cu_{1-x}Fe_xIr_2S_4$ ($x = 0$, 0.01, 0.025, 0.05, 0.1, 0.2, 0.3 and 0.4). The solid and open symbols are for warming and cooling, respectively. The insets of (a) and (b) are the enlargements of the resistivity for $x = 0.1$ and 0.4.

### *3.2. Electrical and magnetic behaviors*

Figures 3 and 4 present the temperature dependence of resistivity and magnetization for $Cu_{1-x}Fe_xIr_2S_4$ ($x = 0$, 0.01, 0.025, 0.05, 0.1, 0.2, 0.3, 0.4), respectively. For $x = 0$, the

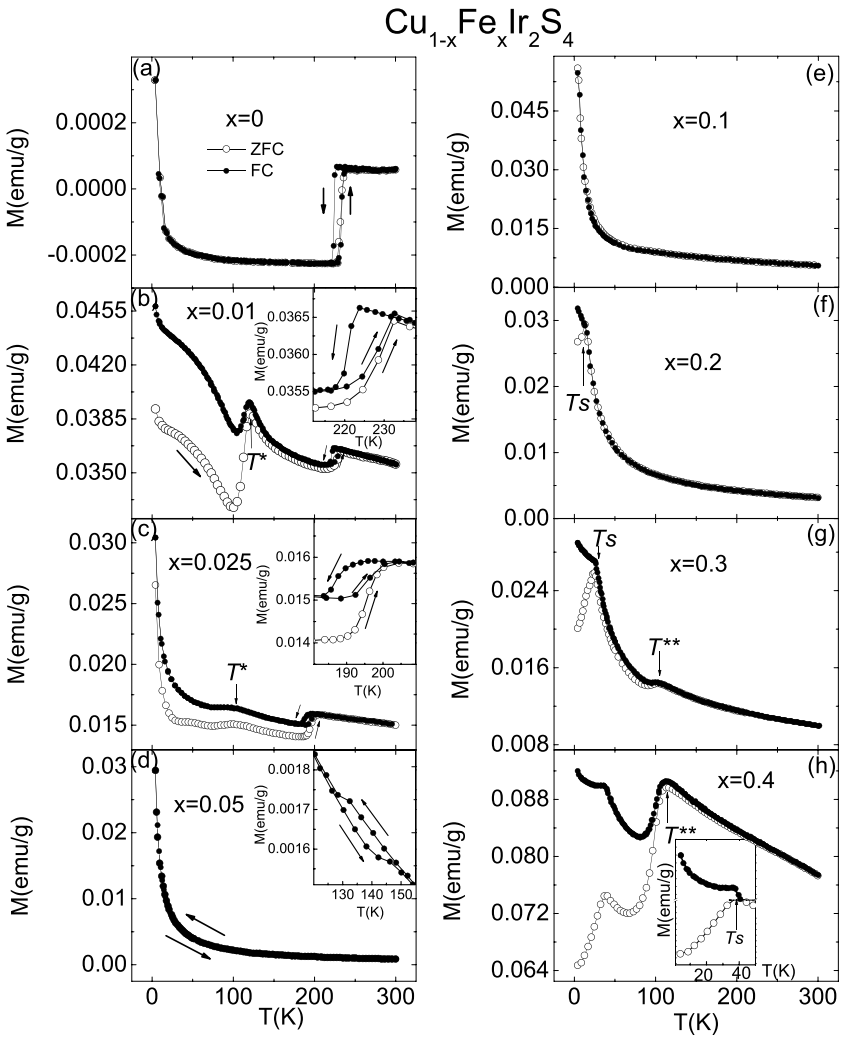


**Figure 4.** The temperature dependence of magnetization for $Cu_{1-x}Fe_xIr_2S_4$ ($x = 0$, 0.01, 0.025, 0.05, 0.1, 0.2, 0.3) measured under $H = 1000$ Oe. The open symbols are for warming under zero field cooling (ZFC), while solid symbols are for warming and cooling under field cooling (FC).

resistivity decreases slightly with cooling when $T > T_{MI}$, indicating that it is in a metallic state. After the Peierls-like phase transition at $T_{MI} \sim 230$ K, the resistivity suddenly increases by about three orders of magnitude, which is shown in figure 3(a). Above $T_{MI}$, the magnetization for $x = 0$ consists of contributions from the Pauli paramagnetism and Larmor diamagnetism (see figure 4(a)). After the Peierls-like phase transition, the free electrons take part in spin-dimerization, resulting in the disappearance of the Pauli paramagnetism, but the Larmor diamagnetism still survives [19]. So the magnetization declines suddenly at $T_{MI}$ and the system shows diamagnetic behavior. Both resistivity and magnetization shows hysteresis at $T_{MI}$, indicating that the transition at $T_{MI}$ is first order.

For $x = 0.01$ and 0.025, the Peierls-like phase transitions are still observed in resistivity and magnetization, which can be seen in figures 3(a) 4(b) and 4(c). The $T_{MI}$ moves to lower temperature, and the jump range in resistivity at $T_{MI}$ becomes smaller with increasing $x$, indicating that the transition is suppressed with the doping of Fe. We note that two unexpected results are observed in the $M$–$T$ curves. First, the magnetization for $x = 0.01$ and 0.025 above $T_{MI}$ is three orders of magnitude larger than that for $x = 0$, and the jump step $\Delta M$ at $T_{MI}$ for $x = 0.01$ and 0.025 is larger than that for $x = 0$. The $\Delta M$ for $x = 0.01$ is the largest. Second, an unexpected transition is detected at $T^* \approx 120$ K for $x = 0.01$ and 100 K for 0.025 respectively, but no corresponding transition is observed in resistivity.

With further increase of $x$, the $T_{MI}$ decreases from 132 K for $x = 0.05$ to 90 K for $x = 0.1$ and the jump in resistivity becomes increasingly weaker, as shown in figure 3(a). This transition is also observed in magnetization for $x = 0.05$ (see the inset of figure 4(d)), but is not observed for $x = 0.1$. Our analysis indicates that the $M$–$T$ behavior for $x = 0.05$ and 0.1 are quite different. As shown in figures 5(a) and (b), the $1/M$–$T$ relation for $x = 0.05$ consists of two straight lines with slightly different slopes above and below $T_{MI}$, which is caused by the reduction of the $Ir^{4+}$ ions owing to the spin-dimerization; while the $1/M$–$T$ curve for $x = 0.1$ is a straight line above 90 K, but it deviates from the straight line below

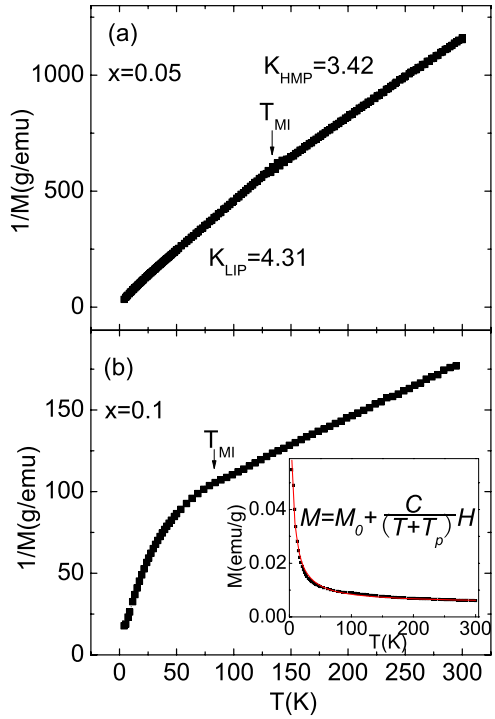


**Figure 5.** The inverse magnetization for $Cu_{1-x}Fe_xIr_2S_4$ for $x = 0.05$ and 0.1 versus temperature. The red curve in the inset of (b) is fitted by the Curie–Weiss law.

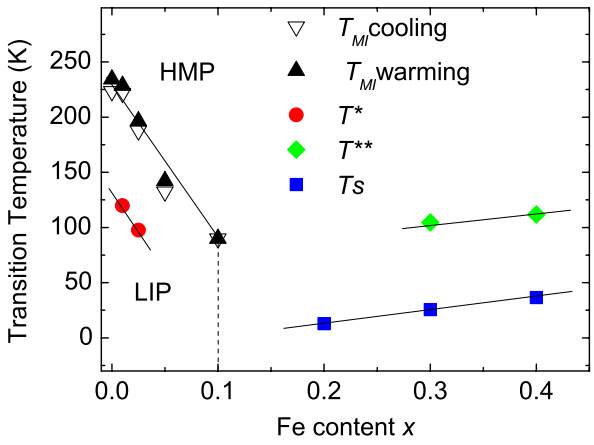


**Figure 6.** The transition temperatures as a function of Fe content $x$.

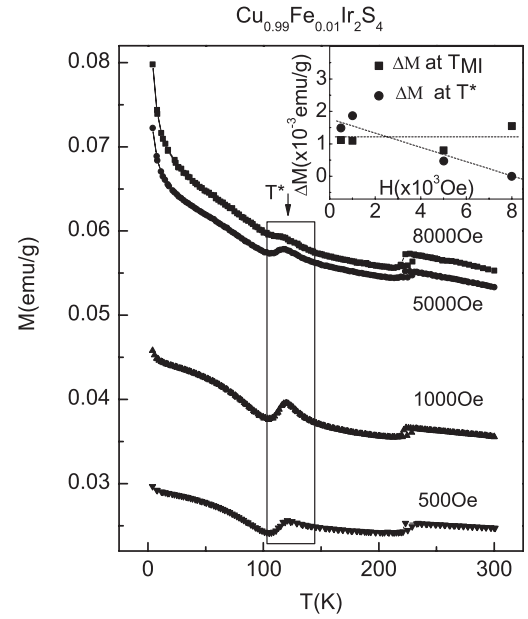


**Figure 7.** The temperature dependence of magnetization for $Cu_{0.99}Fe_{0.01}Ir_2S_4$ under different $H$. The inset is the jump range at $T_{MI}$ and $T^*$ as a function of $H$.

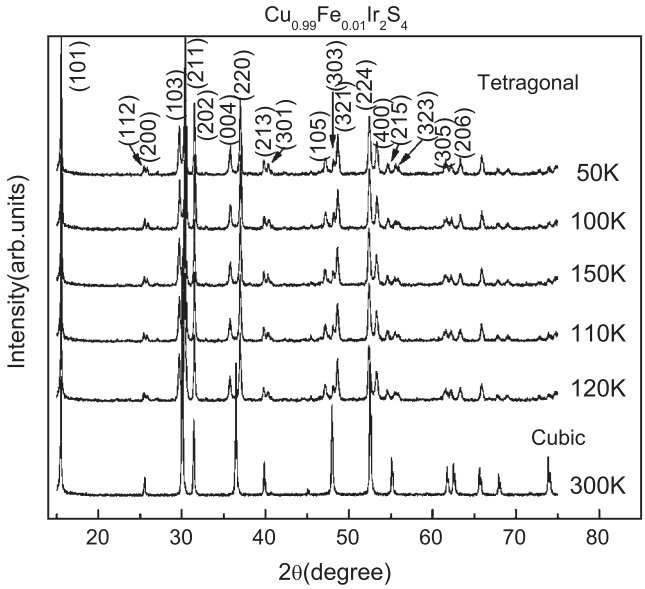


**Figure 8.** Powder x-ray diffraction (XRD) patterns for $Cu_{0.99}Fe_{0.01}Ir_2S_4$ at different temperatures.

90 K. In fact, the $M$–$T$ curve for $x = 0.1$ is well fitted by the Curie–Weiss law:

$$M = M_0 + \frac{C}{T + T_p} H. \quad (1)$$

With the fitting parameters $M_0 = 0.005$ emu g$^{-1}$, $C = 0.00034$ emu K g$^{-1}$, $T_p = 2.49$ K, as shown in the inset of figure 5.

As shown in figure 3(b), the samples with $x = 0.2$, 0.3 and 0.4 show metallic transport behavior, except that there is a small upturn at $T \leqslant 75$ K for $x = 0.4$ (the inset of figure 3(b)). There is no Peierls-like transition for these samples, as seen in figures 3(b) and 4(f)–(h). The λ shape transition which is observed in $M$–$T$ relations under zero field cooling (ZFC) and field cooling (FC) at low temperature, is generally attributed to the occurrence of the cluster–spin-glass state. The λ shape curve for $x = 0.4$ can be made out by raising the ZFC curve to overlap with the FC curve, as shown in the inset of figure 4(h). Another transition at $T^{**} = 100$ K for $x = 0.3$ and 115 K for 0.4 appears in addition to the λ transition in $M$–$T$ relations at lower temperatures. Based on the information presented above, we can construct a phase diagram, which is shown in figure 6.

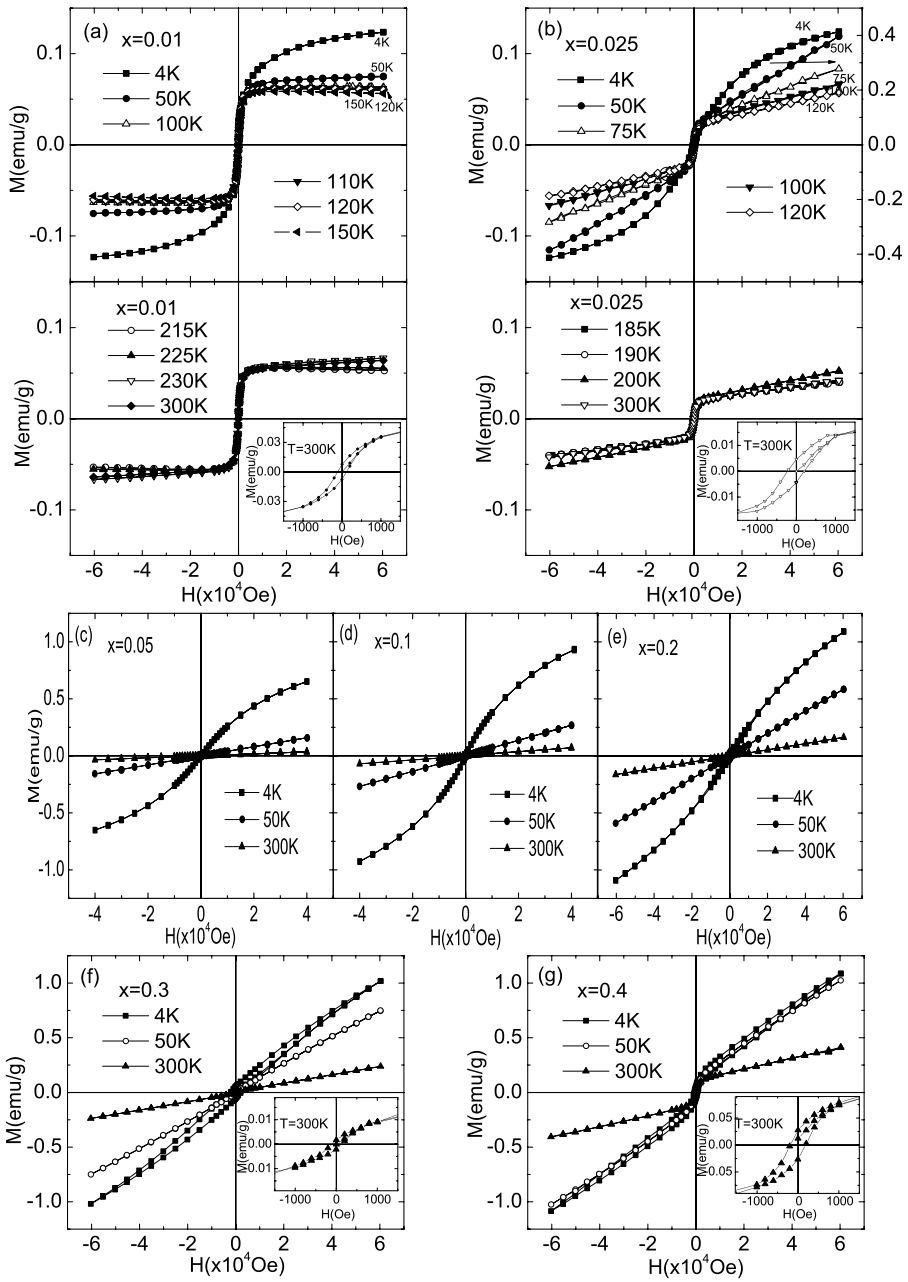


**Figure 9.** The magnetization versus $H$ for $Cu_{1-x}Fe_xIr_2S_4$ ($x = 0.01$, 0.025, 0.05, 0.1, 0.2, 0.3, and 0.4) measured under different temperatures. The insets are enlargements of curves at low field.

### *3.3. Phase transition at $T_{MI}$ and $T^*$ for the low doped samples*

As mentioned above, $M$ and $\Delta M$ at $T_{MI}$ for $x = 0.01$ and 0.025 is larger than that for $x = 0$, and an unexpected transition appears at $T^*$ for $x = 0.01$ and 0.025. In order to understand these phenomena, we perform the $M$–$T$ measurements under different applied magnetic field and XRD at different temperatures for $x = 0.01$.

Figure 7 gives the $M$–$T$ relations for $x = 0.01$ measured under different $H$. One can see that the $\Delta M$ at $T_{MI}$ is hardly changed at different $H$. On the other hand, the transition at $T^*$ is suppressed gradually with increasing $H$, and is totally gone at $H = 8000$ Oe. Figure 8 shows the XRD patterns at different temperatures. It reveals that the Peierls-like transition at $T_{MI}$ is accompanied with a structural change from cubic in HMP to tetragonal in LIP, while the XRD patterns remains unchanged through $T^*$. These results demonstrate that the transition at $T^*$ is not related to a structural transition, but should be a spin transition since it can be suppressed by applied magnetic field.

What causes the large $M$ and $\Delta M$? One possibility is that the $Fe^{2+}$ ion polarizes $Ir^{4+}$ ions with spins around it. In this way, the polarized spins of $Ir^{4+}$ increase $M$. Then, the $\Delta M$ is composed of two parts: (1) the spin-dimerization of $Ir^{4+}$ ions, i.e. the normal Peierls-like phase transition which has not been affected by $Fe^{2+}$; (2) the dimerization of the ferromagnetic (FM) arranged $Ir^{4+}$ ions from the FM arrangement to the AFM arrangement, which causes large $\Delta M$. As discussed above, the

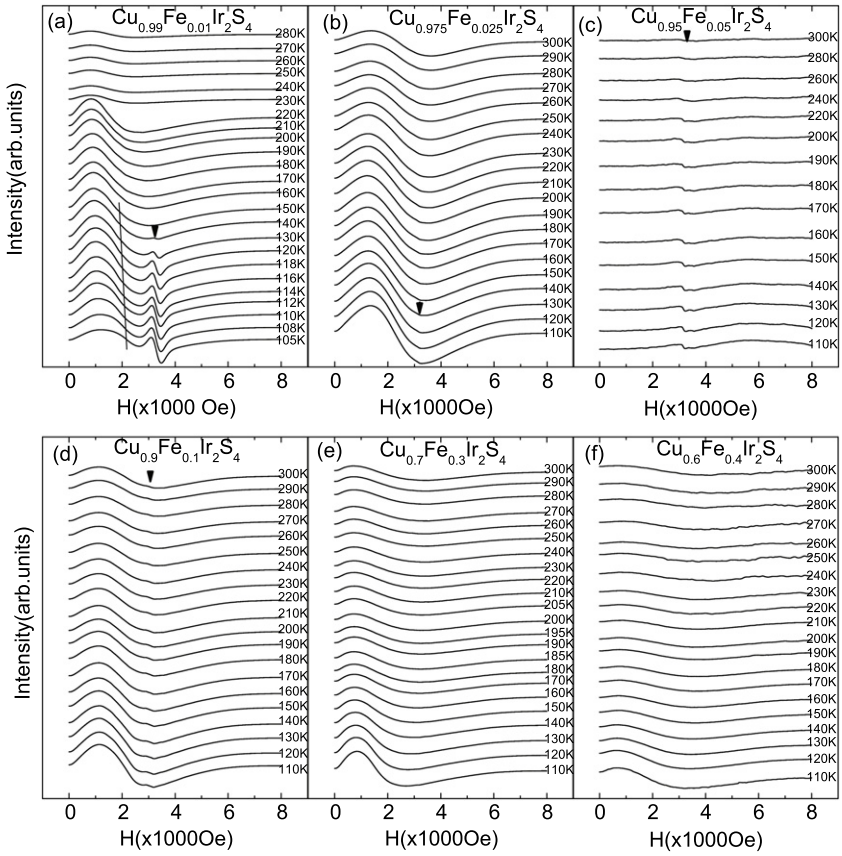


**Figure 10.** The ESR spectra at different temperatures for $Cu_{1-x}Fe_xIr_2S_4$. The symbol ▼ indicates the onset of the PM line.

transition at $T^*$ is a spin transition, which may be caused by the complicated spin coupling between $Fe^{2+}$ and $Ir^{4+}$ ions.

### *3.4. The transformation of FM–PM–FM*

In order to clarify the magnetic state evolution with $x$, $M$–$H$ relations for the doped samples are measured. Figure 9(a) presents $M$–$H$ relations at different temperatures for $x = 0.01$, the inset is the enlarged $M$–$H$ relations at 300 K. All the $M$–$H$ relations for $x = 0.01$ show typical FM characteristics. For the curves at 300 and 230 K above $T_{MI}$, $M$ increases slightly with $H$, which is due to Pauli paramagnetism. For 215 and 225 K just below $T_{MI}$, $M$ decreases slightly with $H$, which is because of the occurrence of the diamagnetism below $T_{MI}$. The behaviors at 50, 100, 110, 120, 150 K are similar to each other, which become saturated with $H$ increasing. The $M$ for 4 K increases with $H$, owing to a few remanent localized electrons exhibiting large Curie paramagnetism at low temperatures. These results indicate that only FM moments dominate from 4 to 300 K. The $M$–$H$ for $x = 0.025$ is similar to that for $x = 0.01$, except that $M$ keeps increasing with $H$ (see figure 9(b)). Figure 9(c), (d) and (e) give the $M$–$H$ relations for $x = 0.05$, 0.1, and 0.2, respectively. For these three samples, the $M$–$H$ relations are very similar; all of them show PM state at 300 and 50 K. Figures 9(f) and (g) show the $M$–$H$ relations at different temperatures for $x = 0.3$ and 0.4, respectively. The magnetic state at 300 K is FM for these two samples (see insets of figures 9(f) and (g)), and the FM magnetization is strengthened with increasing $x$.

The ESR spectra are measured to study the micromagnetism, which is shown in figure 10. For $x = 0.01$ (figure 10(a)), the FM state exists at all temperatures in ESR spectra. Two transitions are detected at 220 and 140 K, corresponding to the transition at $T_{MI}$ and $T^*$. The ESR spectra for $x = 0.025$ is similar to that for $x = 0.01$, except that the intensity is weaker. ESR spectra for $x = 0.05$ (figure 10(c)) only present PM lines, in agreement with the $M$–$T$ behavior. But for $x = 0.1$ (figure 10(d)), FM signals are observed while PM lines become weaker. This indicates that short range ferromagnetism has appeared for $x = 0.1$. Figures 10(e) and (f) show the ESR spectra for $x = 0.3$ and 0.4. Only the FM line could be detected. This suggests that the FM magnetization has been strong for $x = 0.3$ and 0.4.

From $M$–$H$ relations and ESR spectra, it can be seen that the magnetic state transforms from FM ($x = 0.01$ and 0.025) to PM ($x = 0.05$, 0.1, and 0.2) to FM ($x = 0.3$ and 0.4), but short range ferromagnetism has formed for $x = 0.1$. For the low doped samples with $x = 0.01$ and 0.025, the ferromagnetism may come from the spins of $Ir^{4+}$ ions polarized by the $Fe^{2+}$ ions. For the higher doped samples, the magnetic moments of $Fe^{2+}$ play a dominant role. The magnetic moments of $Fe^{2+}$ form cluster–spin glass in the higher doped samples, which result in the cluster–spin glass phase transition at $T_S$. The transition at $T^{**}$ may be due to the interaction of the domains formed by $Fe^{2+}$ ions.

## 4. Conclusion

The $Cu_{1-x}Fe_xIr_2S_4$ ($0 \leqslant x \leqslant 0.4$) system was studied. The Peierls-like phase transition is suppressed completely when $x > 0.1$. A series of changes happen to the electromagnetic behavior, described as follows: (1) there is a large $M$ and $\Delta M$ for $x = 0.01$ and 0.025; (2) an unexpected phase transition appears at $T^*$ for $x = 0.01$ and 0.025; (3) the magnetic state transforms from FM to PM and back to FM with $x$ increasing. The complicated interaction between magnetic moments of $Fe^{2+}$ and $Ir^{4+}$ ions results in the spin transition at $T^*$. With increase of $x$, $Fe^{2+}$ ions form FM domains in highly doped samples, causing cluster–spin glass transition.

## Acknowledgments

The authors would like to thank Professor Yuping Sun (Institute of Solid State Physics, Chinese Academy of Sciences) for the support in sample preparation. This work was supported by the National Nature Science Foundation of China (Nos 10334090 and 10504029), and the State Key Project of Fundamental Research of China (2007CB925001).

## References

[1] Nagata S, Hagino T, Seki Y and Bitoh T 1994 *Physica* B **194–196** 1077–8
[2] Furubayashi T, Matsumoto T, Hagino T and Nagata S 1994 *J. Phys. Soc. Japan* **63** 3333
[3] Burkov A T, Nakama T, Hedo M, Shintani K, Yagasaki K, Matsumoto N and Nagata S 2000 *Phys. Rev.* B **61** 10049
[4] Khomskii D I and Mizokawa T 2005 *Phys. Rev. Lett.* **94** 156402
[5] Yagasaki K, Nakama T, Hedo M, Uwatoko Y, Shimoji Y, Notsu S, Yoshida H, Kimura H M, Yamaguchi Y and Burkov A T 2006 *J. Phys. Soc. Japan* **75** 074706
[6] Ishibashi H, Sakai T and Nakahigashi K 1998 *J. Magn. Magn. Mater.* **226–230** 233
[7] Radaelli P G, Horibe Y, Gutmann M J, Ishibashi H, Chen C H, Ibberson R M, Koyama Y, Hor Y S, Kiryukhin V and Cheong S W 2002 *Nature* **416** 155
[8] Matsuno J, Mizokawa T, Fujimori A, Zatsepin D A, Galakhov V R, Kurmaev E Z, Kato Y and Nagata S 1997 *Phys. Rev.* B **55** R15979
[9] Kumagai K, Tsuji S, Hagino T and Nagata S 1995 *Spectroscopy of Mott Insulators and Correlated Metals* ed A Fujimori and Y Tokura (Berlin: Springer) p 255
[10] Oda T, Shirai M, Suzuki N and Motizuki K 1995 *J. Phys.: Condens. Matter* **7** 4433
[11] Cao G H, Furubayashi T, Suzuki H, Kitazawa H, Matsumoto T and Uwatoko Y 2001 *Phys. Rev.* B **64** 214514
[12] Cao G H, Suzuki H, Furubayashi T, Kitazawa H and Matsumoto T 2000 *Physica* B **281** 636–7
[13] Yagasaki K, Nakama T, Hedo M, Uchima K, Shimoji Y, Matsumoto N, Nagata S, Okada H, Fujii H and Burkov A T 2002 *J. Phys. Chem. Solids* **63** 1051
[14] Cao G H, Xu X F, Jiao Z K, Kitazawa H, Matsumoto T and Feng C M 2005 *Phys. Rev.* B **72** 125128
[15] Cao G H, Kitazawa H, Matsumoto T and Feng C M 2004 *Phys. Rev.* B **69** 045106
[16] Nagata S, Asakura T and Awaka J 2004 *J. Magn. Magn. Mater.* **272–276** 392
[17] Endoh R, Matsumoto N, Chikazawa S, Nagata S, Furubayashi T and Matsumoto T 2001 *Phys. Rev.* B **64** 075106
[18] Binder H 1973 *Z. Naturf.* b **28** 256
[19] Zhang L, Ling L S, Tan S, Pi L and Zhang Y H 2008 *J. Phys.: Condens. Matter* **20** 255205